

The Study of Cylindrical Polymer Fuel Cell's Performance and the Investigation of Gradual Geometry Changes' Effect on Its Performance

Hossein Samanipour^{1*}, Nima Ahmadi², Iraj Mirzaee¹, Majid Abbasalizade¹

¹ Department of Mechanical Engineering, Faculty of Engineering, Urmia University, 11 km Sero Road, 57561-51818 Urmia, Iran

² Department of Mechanical Engineering, Faculty of Mechanical Engineering, Urmia University of Technology, 2 km Band Road, 57166 -17165 Urmia, Iran

* Corresponding author, e-mail: samanipour2002@gmail.com

Received: 03 July 2018, Accepted: 15 October 2018, Published online: 28 January 2019

Abstract

To achieve an optimal perception of cardinal processes and prior to prototype fabrication to fuel cell optimization, modeling is extensively used in industrial researches and applications to transfer mass and heat into small-sized channels. In the current study, Computational Fluid Dynamics is presented to cylindrical polymer fuel cell with circular and elliptical cross-section. Concurrently, the design of fractured electrode-membrane assembly is introduced. The simulations explicitly demonstrate comparing to Base case production, the fractured case of the Electrode Membrane Assembly produces more current. Likewise, a new design for cylindrical polymer fuel cell is illustrated. In the cylindrical design, both the effect of gradual geometric changes on the performance including radius changes and the transformation of cross-section from circle to ellipse has been investigated and compared to Base case. The obtained results displays the cylindrical fuel cell's better performance compared to Base case. Accordingly, establishing wider passage, in same volume for reactive gases toward reaction areas, results in sharp increase in the performance. Finally, validating simulation with valid laboratory results, proper correspondence is achieved.

Keywords

circular, Computational Fluid Dynamics, polymer fuel cell, electrode membrane assembly

1 Introduction

The proton membrane fuel cell, a novel future energy source, applying a polymer membrane as electrolyte, has attracted intense attention chiefly for transportation and residential purposes [1]. The current fuel cell carries considerable advantages including; high efficiency, noiselessness and compliance with environmental standards, low temperature operation, fast start up, no liquid electrolyte and simple design [2]. Nonetheless, prior competing with old combustion plants, it needs to be optimized both in efficiency and costs [3, 4].

In recent years, research and development on fuel cells and systems have extensively accelerated, however the costs of fuel cell system is still too high to turn it to a long lasting commercial product [5]. In a fuel cell, fuel (such as hydrogen gas) and oxidizing (such as oxygenated gas from the air) are taking to generate electricity, while the fuel cell performance generates products like water and heat [6, 7]. Simply put, a fuel cell generally works with these rules: as hydrogen gas

flows into fuel cell on anode side, a platinum catalytic layer facilitates the oxidation of hydrogen gas leading to the production of proton (hydrogen ion) and electron. Meanwhile hydrogen ions are directly transferring to a membrane (part at the center of the fuel cell which separates cathode and anode) and anew with catalytic layer's assistance combine with oxygen and electrons to produce water [8]. The electron unable to pass membrane directly, taking external electric circuit including a motor or other electrical system has to flow from anode to cathode [9].

Both porous anode and cathode electrodes are constructed of electrical conductive materials, regularly carbon [10]. Moreover, the outer part of the electrodes is in contact with membrane consisting carbon, polymer electrolyte and platinum-based catalyst [11]. The half-reaction of oxidation and reduction of fuel cell occurs in active layers of anode and cathode, respectively [12]. Additionally, fuel cell electrodes are infiltrative gas flow and generally designed

for maximum surface area per unit volume (specific surface) [13]. In the present method, the accessibility of gas emission layer is provided to minimize transfer resistance of hydrogen and oxygen to active layers of reaction [14].

In the past decade, extensive research efforts have been taken to develop reality based simulations [15]. Furthermore, researchers all over the world have concentrated on fuel cell system optimization. Regarding cost, they targeted to put it compatible to existing energy converters [16].

Multitude studies have taken diverse functions of polymer fuel cell as subsidiary of its operative conditions. The numerical modeling, which has considerable application in studies related to principal phenomena going in the fuel cell system, is essentially applied in the present study [17].

Needless to say countless researches have been made to improve polymer fuel cell performance. Many parameters such as temperature, pressure, humidification of gas flow and other geometric parameters define the functionality of polymer fuel cell. Geometric parameters play a chief role to affect the performance of polymer fuel cells. To take an example, the cell performance with lower shoulder width (bipolar plate width ratio) is better than the larger shoulder width models [18]. Additionally, one of determinant factors, which have assigned a lot of studies, is the effect of gas channels geometry on the performance of polymer fuel cells. Here the geometry effect of two rectangular and trapezoidal channels was numerically simulated and then the results were analogized. The results demonstrate the rectangular geometry produces more current at the same voltage [19]. Likewise, Ebrahimi et al. [20] studied the effect of uniform distribution of non-homogeneous catalytic layer on the performance of fuel cell. Their two-dimensional and numerical study points out that with optimal distribution of cathode catalytic layer, the performance of the cell will increase by about 7%. The same way Cooper et al. [21] investigated particle coefficient changing effect on the polymer fuel cell performance with the interconnected gas channels. Also, Yan et al. [22] simulated mass transfer event in quite unstable status for a polymer fuel cell. Similarly, a study conducted by Liu et al. [23] demonstrated two dimensional analytical models for polymer fuel cell. Ahmadi et al. [24] taking perturbation method presented an analytical model for cylindrical polymer fuel cell. Having solved the equations of continuity and momentum, they found out the velocity distribution in gas channel [25]. Concurrently they studied and modeled transmission of species in polymer fuel cell.

Noting that fuel cells are generally come with square-shaped channels, the present study attempted to accurately

peruse geometric changes effect on polymer fuel cell's performance. Accordingly, a polymer fuel cell design with fractured electrode membrane assembly is initially introduced. Then, cylindrical polymer fuel cell, as completely novel design is presented and finally after studying its full performance compared with Base case. In present work the cylindrical PEMFC is modeled numerically in more detail and new design especially for the cathode and anode gas channels is presented too which is differ from the Ahmadi et al.'s work [24]. All of the results for cylindrical cases have compared to the results of conventional design of PEMFC with rectangular cross section. In addition, in this work a two phase model is presented to simulate the effect of various designs on the liquid water (water saturation). Also in this work new design for assembling the MEA (deflected MEA) for the Base model is proposed.

2 Mathematical Model

In the present study, Fig. 1 illustrates computational domain as well as network. Noting that cell comprises hydrogen and oxygen channels, bipolar plates both on anode and cathode side comprised of cell and electrodes and membrane are both located between gas channels.

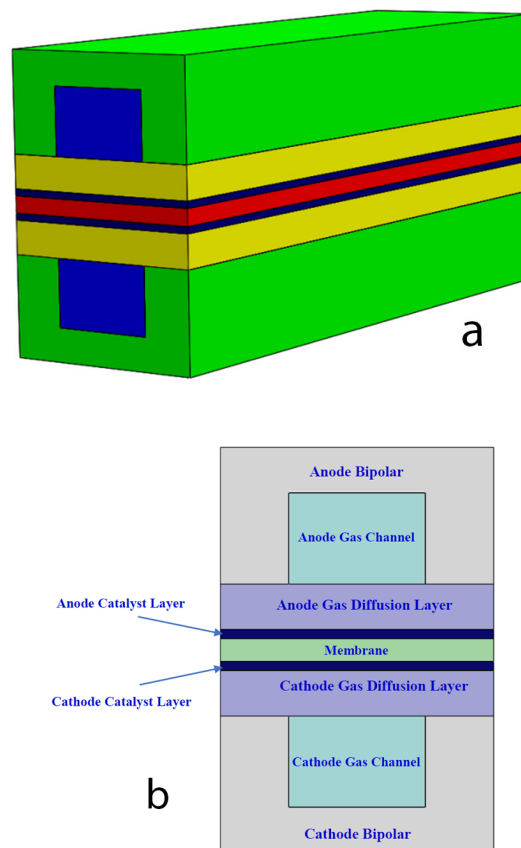


Fig. 1 Fuel Cell Overview (Computational domain).

3 Model Assumptions

In the present non-isothermal model, some simplifications are implemented. The gas intermixing is thought to be ideal, both gas permeation and porous catalytic layer are homogeneous, the current is incompressible and laminar and finally because of smallness of velocity and Reynolds number (less than 200), the model is laminar and incompressible.

4 Governing Equations

In this numerical simulation, the following dominant equations are operated. The momentum mass conservation and equations of Species are as follow [1]:

$$(\nabla \cdot \rho \mathbf{u}) = 0 \quad (1)$$

$$\frac{1}{(\varepsilon_{eff})^2} \nabla \cdot (\rho \mathbf{u} \mathbf{u}) = -\nabla P + \nabla \cdot (\mu \nabla \mathbf{u}) + S_u \quad (2)$$

$$\nabla \cdot (\mathbf{u} C_K) = \nabla \cdot (D_K^{eff} \nabla C_K) + S_K \quad (3)$$

$$\nabla \cdot (\kappa_e^{eff} \nabla \Phi_e) + S_\Phi = 0 \quad (4)$$

In Eq. (1), ρ is density of gas mixture. ∇ is the vector differential operator. According to model's assumptions, source of mass is ignored. ε is effective porosity inside porous layers and μ is viscosity of gas mixture in momentum equation which is demonstrated in Eq. (2). The term momentum source, S_u , is used to describe Darcy's drag to flow through gas permeation and catalytic layer [26]:

$$S_u = -\frac{\mu}{K} \mathbf{u} \quad (5)$$

In Eq. (5), K is permeability of gas inside porous environment. In Species eq. indicated in Eq. (3), effective penetration coefficient is K Species (such as hydrogen, oxygen, nitrogen and water vapor). It is proposed by Bragman to describe the porosity effects on porous gas penetration and catalytic layer [27]:

$$D_K^{eff} = (\varepsilon_{eff})^{1.5} D_K \quad (6)$$

Moreover, diffusion coefficient is operation of pressure and temperature [28]:

$$D_K = D_K^0 \left(\frac{T}{T_0}\right)^{\frac{3}{2}} \left(\frac{P_0}{P}\right) \quad (7)$$

Species transfer properties are given in Table 1.

Equation (4) is load conservation equation. In this equation, K_e is ion conduction in ion metric phase. It's necessary to add that it is recorded by Springer et al. [29]:

$$\kappa_e = \exp\left[1268\left(\frac{1}{303} - \frac{1}{T}\right)\right] \times (0.005139\lambda - 0.00326) \quad (8)$$

Table 1 Transitional properties of the species [28].

| Quantity | value |
|-----------------|---|
| $D_{H_2}^0$ | $1.1 \times 10^{-4} \text{ m}^2/\text{s}$ |
| $D_{O_2}^0$ | $3.2 \times 10^{-5} \text{ m}^2/\text{s}$ |
| $D_{H_2O}^0$ | $7.35 \times 10^{-4} \text{ m}^2/\text{s}$ |
| $D_{H_2}^{mem}$ | $2.59 \times 10^{-10} \text{ m}^2/\text{s}$ |
| $D_{O_2}^{mem}$ | $1.22 \times 10^{-10} \text{ m}^2/\text{s}$ |

In addition, in recent equation, λ could be defined as number of water molecules in each group of sulfonate inside membrane. The amount of water can be taken as a function of water activity and is determined by experimental data [30]:

$$\lambda = 0.3 + 6a[1 - \tanh(a - 0.5)] + 3.9\sqrt{a} \left[1 + \tanh\left(\frac{a - 0.89}{0.23}\right)\right] \quad (9)$$

Water activity is determined by Eq. (10):

$$a = \frac{C_w RT}{P_w^{sat}} \quad (10)$$

The proton conduction in the catalytic layers is introduced by Bragman's relation [27]:

$$\kappa_e^{eff} = \varepsilon_m^{1.5} \kappa_e \quad (11)$$

In recent equation, ε_m is volume fraction of the membrane phase in catalytic layer. Source terms of Eq. (3) and Eq. (4) is provided in Table 2. The localized current density in the membrane is calculated by Eq. (12) [29, 31]:

$$I = -\kappa_e \nabla \Phi_e \quad (12)$$

Then average flow density is calculated as:

$$I_{ave} = \frac{1}{A_{A_{mem}}} \int IdA \quad (13)$$

In recent relation, A is the effective area of electrode assembly reaction.

The energy equation can be introduced as follow:

$$\rho c_p \mathbf{u} \cdot (\nabla T) = \nabla \cdot (k_{eff} \nabla T) + S_T \quad (14)$$

In Eq. (14) c_p is specific heat capacity of reactant gases, k_{eff} is effective thermal conductivity of gases and S_T is the source term of energy equation [25].

5 Boundary conditions and Solving Methods

The supposed boundary conditions of study are presented in Table 2 [32]. According to momentum conservation equation, fuel and air velocity is determined at inlets of anode and cathode gas channels. The stoichiometry concept obtains values of velocities (stoichiometry is essentially the ratio amount of input fuel to amount of fuel needed in one Amp current).

Table 2 Boundary conditions in polymer fuel cell [32].

| Place in the fuel cell geometry | Type of boundary condition |
|---|---|
| Anode channel inlet | $u = u_{in}, T = T_{in}, v = 0,$ $C_{H_2} = C_{H_2,in}^a, C_{H_2O} = C_{H_2O,in}^a$ |
| Cathode channel inlet | $u = u_{in}, T = T_{in}, v = 0,$ $C_{O_2} = C_{O_2,in}^c, C_{N_2} = C_{N_2,in}^c$ |
| Anode and Cathode channel outlet | $\frac{\partial u}{\partial x} = \frac{\partial v}{\partial x} = \frac{\partial w}{\partial z} = \frac{\partial T}{\partial x} = 0$ |
| Interface of gas channels and GDLs | $\frac{\partial u}{\partial y} = \epsilon_{eff,GDL} \frac{\partial u}{\partial y} = \epsilon_{eff,GDL} \frac{\partial u}{\partial y}$, $\frac{\partial v}{\partial y} = \epsilon_{eff,GDL} \frac{\partial v}{\partial y} = \epsilon_{eff,GDL} \frac{\partial v}{\partial y}$, $\frac{\partial w}{\partial y} = \epsilon_{eff,GDL} \frac{\partial w}{\partial y} = \epsilon_{eff,GDL} \frac{\partial w}{\partial y}$ |
| Interface of GDLs and catalyst | $\epsilon_{eff,GDL} \frac{\partial u}{\partial y} = \epsilon_{eff,CL} \frac{\partial u}{\partial y}$, $\epsilon_{eff,GDL} \frac{\partial v}{\partial y} = \epsilon_{eff,CL} \frac{\partial v}{\partial y}$, $\epsilon_{eff,GDL} \frac{\partial w}{\partial y} = \epsilon_{eff,CL} \frac{\partial w}{\partial y}$ |
| Interface of catalyst and membrane | $u = v = w = C_i = 0$ |
| Upper surface of gas channels | $u = v = w = C_i = 0,$ $T_{surface} = 353K$ |
| Lower surface of gas channels | $u = w = 0, T_{surface} = T_{wall}$ |
| Upper surface of anode bipolar plates | $\phi_{sol} = 0, \frac{\partial \phi_{mem}}{\partial y} = 0$ |
| Upper surface of cathode bipolar plates | $\phi_{sol} = V_{cell}, \frac{\partial \phi_{mem}}{\partial y} = 0$ |
| External surfaces | $\frac{\partial \phi_{mem}}{\partial x} = 0, \frac{\partial \phi_{mem}}{\partial z} = 0,$ $\frac{\partial \phi_{sol}}{\partial x} = 0, \frac{\partial \phi_{sol}}{\partial z} = 0$ |

An in-house code is developed by using FORTRAN software to solve the governing equations. To discretizing the governing equations, finite volume scheme in the implicit formation is utilized. Afterwards, the pressure-velocity linked equations are solved numerically using The SIMPLE algorithm [33]. Reduplicative algorithm is used to solve extracted algebraic equations. The calculations are frequently taken in each time step in order to the convergence criterion is fulfilled. If the residuals of iterations are reached to less than 10^{-9} , it can be expected

that the convergence be obtained. For the numerical simulating, structured computational cells of grid are generated. The system that is used for numerical procedure is the IBM quad core (2.4 GHz) PC. The mean time for convergence the solution is about 12 hours.

Formula to fuel rate entering anode channels is achieved through Eq. (15) [32]:

$$u_{an} = \frac{\zeta}{X_{H_2,in}} \frac{I_{avg}}{2F} \frac{RT_{in}}{P_{in}} \frac{A_{MEA}}{A_{ch}}$$

$$u_{cat} = \frac{\zeta}{X_{O_2,in}} \frac{I_{avg}}{4F} \frac{RT_{in}}{P_{in}} \frac{A_{MEA}}{A_{ch}}$$
(15)

In presented formula ζ is anode side stoichiometry, $X_{H_2,in}$ volume fraction of input hydrogen, I_{avg} reference flow density which equals to $I = 15000 \text{ A/m}^2$, R gas global constant, F Faraday number, T_{in} and P_{in} , input temperature and gas pressure to anode gas channel, respectively, A_{MEA} area for active fuel cell surface and finally A_{ch} anode sectional area of channel.

6 Results and discussion

6.1 Model validation

In order to verify accuracy of model, the numerical simulation results (for parallel current or Base model channel) are compared with experimental data provided by Wang et al. [32] and Ahmadi et al. [25], shown in Fig. 2. As it is obvious, acceptable compliance is caught between numerical model and experimental data. The power density curve for numerical model is illustrated as well. As specifically determined, the relationship between voltage, current density and fuel cell power is accountable by relation $P = V \times I$. Minor difference in 0.4 V voltage is specified in single-phase mode. Insomuch, single-phase model is incapable to spot effects of liquid water, therefore density drops in such voltages are not well modeled. However, the multiphase model has supreme compliance with experimental

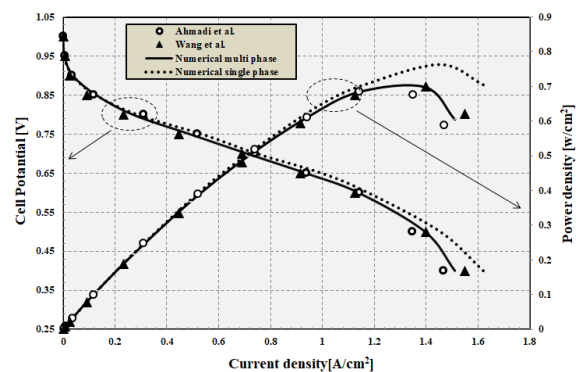


Fig. 2 Polarization and power density diagrams.

results. Thereupon, validating Base model, geometric changes effect on cell performance are studied.

The operational state of fuel cell and its geometric parameters are shown in Table 3. Noting that the input gases on both sides, the anode and cathode are fully in humid state.

The present study attempts to demonstrate the analogy between two fuel cells; square-channel and cylindrical. Concurrently, geometrical changes' effect on cell performance is studied as well. The meshing Base model by front facade is illustrated in Fig. 3.

Fig. 4 marks the testing result for independence of mesh. As it is displayed, picking up 200000 computational cells and increasing number of mesh cells, there is no change in density of fuel cell outflow. They stay stable and consequently numerical results are independent of cells number.

Table 3 Geometrical and operational parameters of cell.

| Parameter | Symbol | Value | Unit |
|---|----------------|-------------------------|------|
| Channel length | L | 0.05 | m |
| Channel width | W | 3×10^{-3} | m |
| Channel height | H | 3×10^{-3} | m |
| Land area width | W_{land} | 3×10^{-3} | m |
| Gas diffusion layer thickness | d_{GDL} | 0.26×10^{-3} | m |
| Wet membrane thickness (Nafion 117) | δ_{mem} | 0.23×10^{-3} | m |
| Catalyst layer thickness | δ_{CL} | 0.0287×10^{-3} | m |
| Anode pressure | P_a | 3 | atm |
| Cathode pressure | P_c | 3 | atm |
| Inlet fuel and air temperature | T_{cell} | 353.15 | K |
| Relative humidity of inlet fuel and air (fully humidified conditions) | ψ | 100 | % |

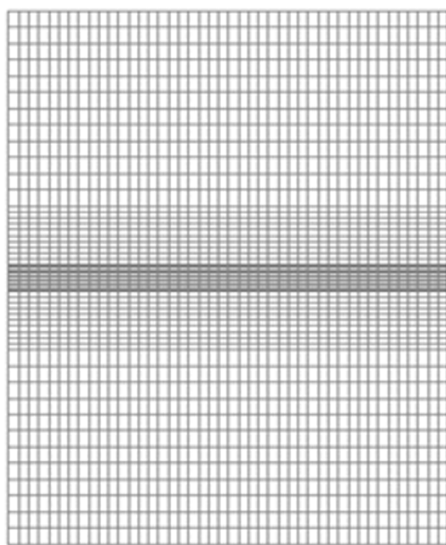


Fig. 3 The shape of the meshing model from the front view.

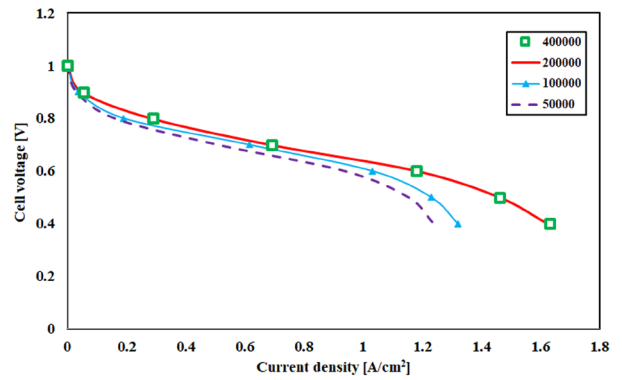


Fig. 4 Independence test of mesh for polarization diagram.

Likewise, Fig. 5 indicates the localized grid independence test, which is shown for oxygen mole fraction along the cathode catalyst layer.

The present research, initially, investigates geometric changes effect in electrode membrane assembly and afterwards through modeling cylindrical fuel cell, studies its effect on cell performance.

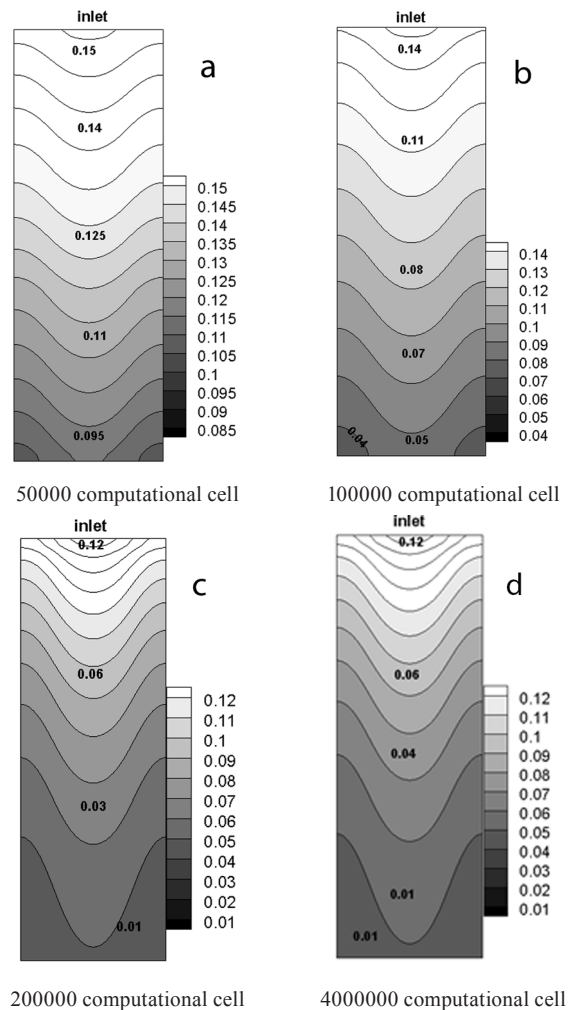


Fig. 5 Oxygen mole fraction along the cathode catalyst layer for the different number of mesh cells.

6.2 The study of geometric changes effect and operating conditions on polymer fuel cell performance

6.2.1 Creation of deflection in electrode membrane assembly

Fig. 6 represents a schematic diagram of created deflection both in electrode and membrane assembly in polymer fuel cell which is compared with Base case. Table 4 displays geometric characteristics of new arrangement for electrode membrane assembly in two cases including upward and downward fracture formation which again compared with Base case.

Fig. 7 shows polarization diagram for both upward and downward deflection modes compared to Base case. It is quite obvious that downward deflection mode has produced a higher current density than two other states.

Fig. 8 compares the production rate of cross-sectional current intensity for three different modes. The reason why the deflection mode produces more current than Base case relies in the area. In other words, the area for electrode membrane assembly is more than Base case and so qualitatively and quantitatively results in better transmission of reactive forms toward the reaction area. Also downward deflection (fracture toward cathode) case has better performance compared to the other cases. Likewise, since area for electrode membrane assembly in the same width is large, therefore; the higher the area toward reaction areas (located on catalyst side of cathode), the better the cell performance. As it is expected, the formation of downward deflection provides an appropriate ground to transfer reactive gases.

Fig. 9 displays cell's cross-sectional distribution of mass fractional oxygen to cell's input and output. As it is seen, the amount of oxygen consumption is much higher in shoulder region (fractured regions). Interestingly enough in middle points the amount of oxygen consumption is almost equal in three cases.

Fig. 10 indicates the distribution of molar fraction of oxygen at cathode channel's floor in 3 cases. It is observed that downward deflection case experiences higher oxygen

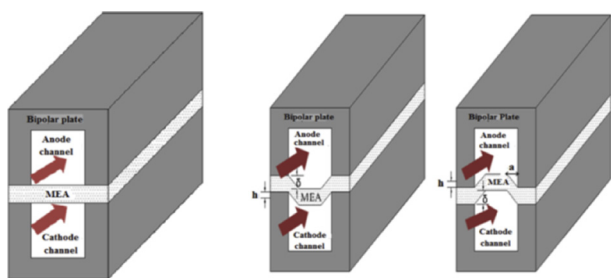


Fig. 6 The schematic diagram of fracture creation in electrode membrane assembly compared with Base model (left side).

Table 4 The geometric properties of new arrangement for electrode membrane assembly

| cases | $a = \delta$ (mm) | h (mm) |
|---------------------|-------------------|----------|
| Base | 0 | 0 |
| upward deflection | 0.25 | 0.1875 |
| downward deflection | 0.25 | 0.1875 |

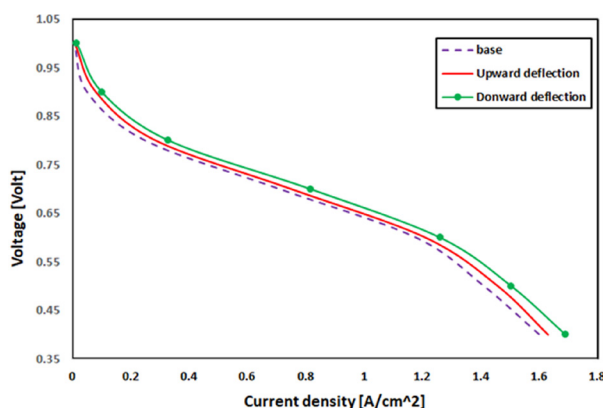


Fig. 7 Comparison of polarization diagram for three cases.

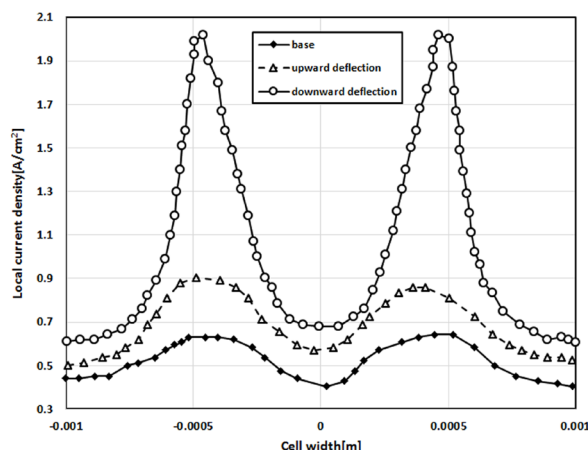


Fig. 8 Comparison of the production amount of current intensity in cross-sectional for three cases.

consumption due to higher performance. Therefore, the presence of oxygen at cathode channel's floor is less than the other two cases.

6.2.2 Cylindrical fuel cell Modeling

6.2.2.1 Cylindrical fuel cell with circular cross section

This section simulating cylindrical polymer fuel cell, compares its performance with Base case of (with square gas channel) fuel cell (Fig. 11 a). Three plans are presented for cylindrical fuel cell. The first is (case A) circular cross section. At second stage the gradual changes effect in total shape of fuel cell is studied. Having kept the total volume and size of various parts of pill stable in Fig. 11 b, cell is

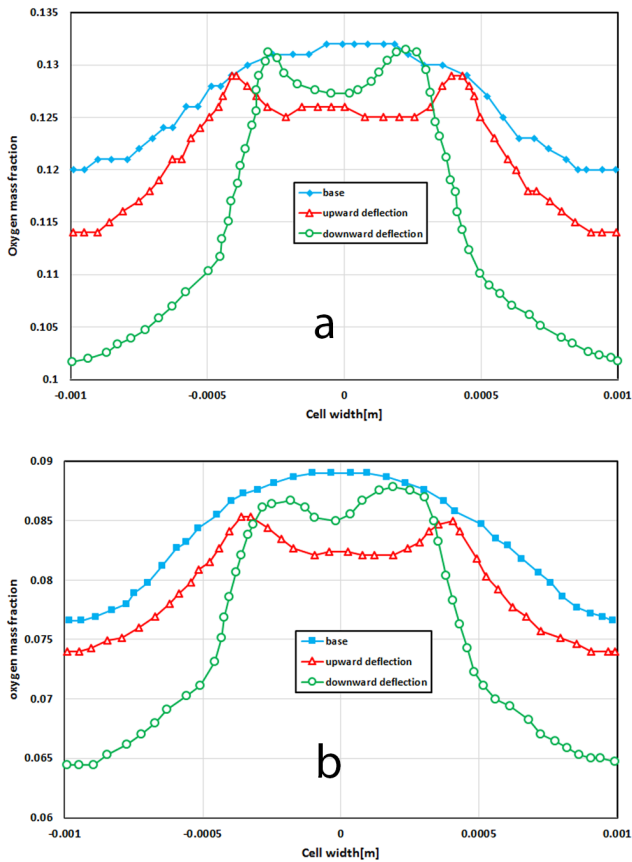


Fig. 9 The distribution of oxygen mass fraction in cross section of cell to input (a) and output (b) of the cell.

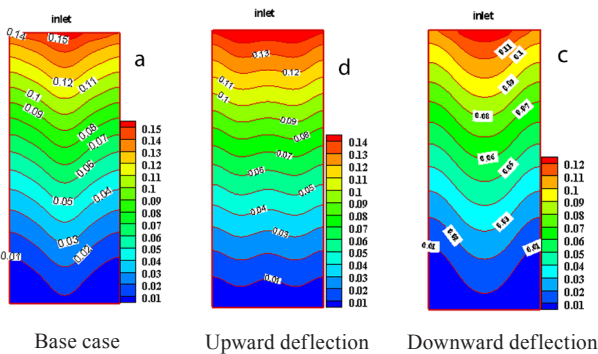


Fig. 10 The distribution of oxygen mole fraction at cathode gas channel's floor in three cases.

converting to elliptical cross sectional fuel cell. To convert circle cross section to elliptical one, the total volume and size of various parts of cell should be kept stable, meanwhile vertical radius (which turns into a small ellipse diameter) reduces around 20 % and horizontal radius gets larger (20 %) to keep the total volume of cell and other dimensions stable. This plan case is nominated as case B (Fig. 11 c). In following step, plan three, introduced as case C (Fig. 11 d), only vertical radius in case A

decreases by 20 % and horizontal radius stays stable. Here, the length of fuel cell is precisely same as cases A and B. Fig. 11 displays recent plans compared to Base case.

The geometric characteristics of cylindrical fuel cell from front view are shown in Fig. 12.

Table 5 presents compared geometric specifications of various cases, dimensional and geometric, with Base case. It should be noted that other operational characteristics of cell in various cases are similar to Base case and have not changed.

Fig. 13 illustrates both polarization diagram and power density for various cylindrical fuel cell cases which again are analogized with Base case.

As it is displayed, all various modes of cylindrical design produce more output current compared to Base case. Meanwhile, case B produces the most and case C the least amount of current intensity. Fig. 14 shows the contour density distribution of current intensity for all cases (Voltage 0.4 V) compared to Base case.

As shown in Fig. 14, the cylindrical design shows a significant increase in performance compared to Base case. It is worth mentioning that the principal factor to evaluate

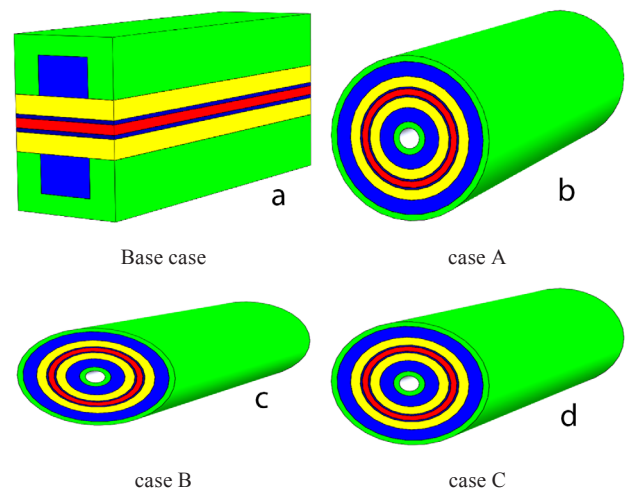


Fig. 11 3D view of proposed designs.

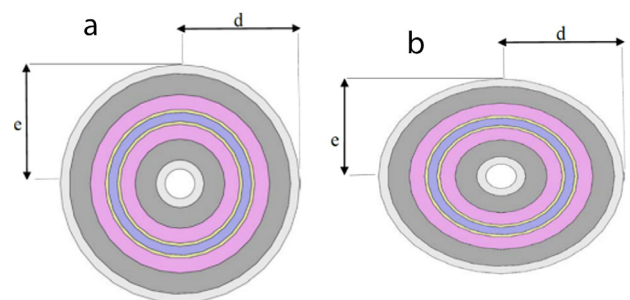


Fig. 12 Front view of the cylindrical fuel cell with circular and elliptical cross section.

Table 5 Dimensional specification of various cases.

| Parameter | Base | A | B | C |
|---|--------|--------|--------|--------|
| Gas channel length (L) (mm) | 50 | 8.95 | 8.95 | 8.95 |
| Diffusion layer thickness (δ_{GDL}) (mm) | 0.26 | 0.26 | 0.26 | 0.26 |
| Catalyst layer thickness (δ_{cl}) (mm) | 0.0287 | 0.0287 | 0.0287 | 0.0287 |
| Membrane thickness (δ_{mem}) (mm) | 0.23 | 0.23 | 0.23 | 0.23 |
| Gas diffusion layer porosity (ϵ_{GDL}) | 0.4 | 0.4 | 0.4 | 0.4 |
| Membrane porosity (ϵ_{mem}) | 0.4 | 0.4 | 0.4 | 0.4 |
| Horizontal radius (d) (mm) | --- | 3.8074 | 4.5689 | 3.8074 |
| Vertical radius (e) (mm) | --- | 3.8074 | 3.046 | 3.046 |

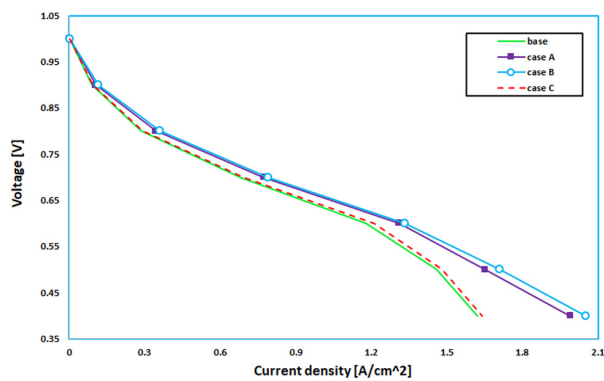


Fig. 13 The Comparison of polarization graph for various cases.

fuel cell performance is output current intensity in cell. The cylindrical design, on the one hand, provides highly appropriate ground to get optimal and monotonous flow of reactive gases to reaction regions close to cathode catalytic layer and membrane. On the other hand, in cylindrical design, in an analogy between electrode and membrane effective area and Base case, area size of reactor gas passage from gas channel floor to reaction regions along the channel is significantly increased. Thus, again keeping comparison with Base case, the reactive gases penetrate so much better and quite monotonously into the reaction areas. This phenomenon is substantially impressive in case B. It relies in increasing length in horizontal part d , since the higher the increase area in reactor passage from channel floor, the higher the passing of gas reach to reaction areas. However, comparing with two other cases, in case C, at the same input mass for reactors, the gas channel input area is slightly reduced. Hence, the speed of anode and cathode gas channels will be higher than the

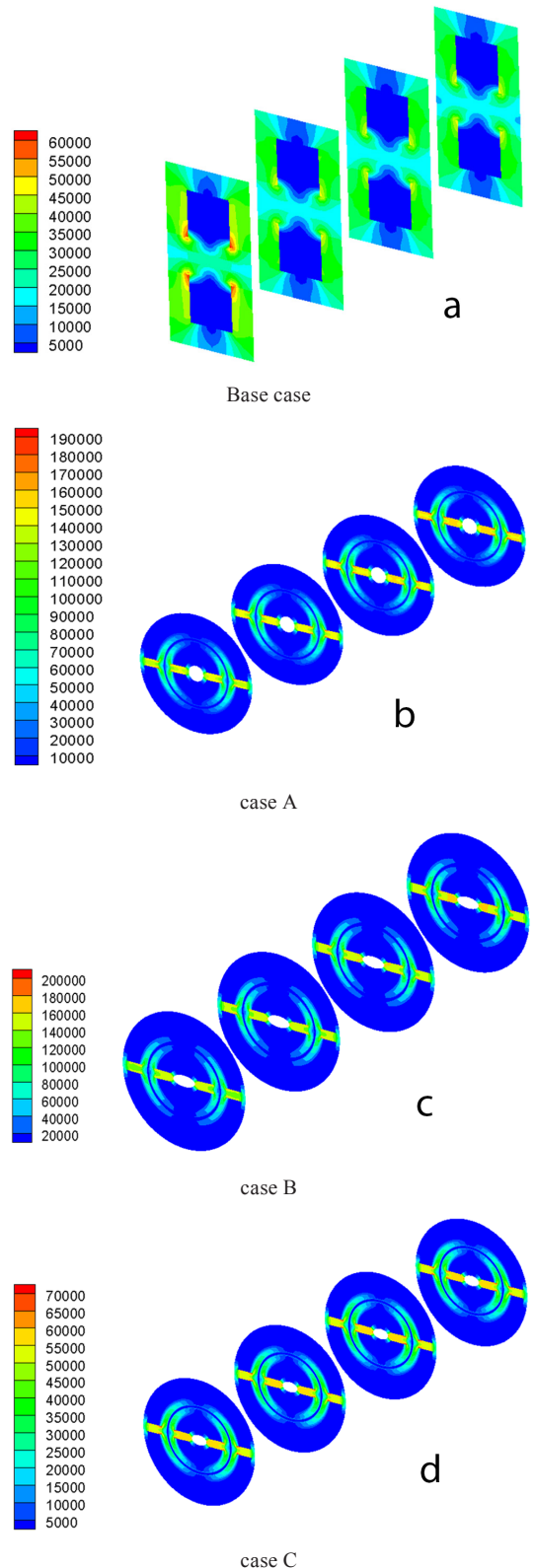


Fig. 14 The comparison of output current intensity for various cases.

other two. Increasing the velocity, if other parameters stay stable, results in power enhancement for momentum displacement compared to mass penetration, and thereupon the amount of mass penetration to reaction regions reduces and consequently performance rate significantly falls. The penetration rate of reactant gases is higher in case B and lowest in case C.

Fig. 15 illustrates velocity distribution rate along fuel cell for various cases. According to Fig. 15, it is quite clear the velocity, especially in cathode channel of case C is more than the other two cases. In Base case, the speed rate, chiefly in cathode gas channel, is much higher than cylindrical case. Therefore, this case carries lower performance rate than cylindrical cell. Fig. 16 displays the rate of oxygen mass fraction at cathode side for various cases. The oxygen rate perceptibly falls due to consumption both in cathode side along fuel cell and current direction.

Fig. 16 distinctly displays higher oxygen consumption in both A and B cases than to other cases. The chief reason discerned for high oxygen consumption is heavy current rates. Hence, in the cell's end regions at these cases, the oxygen concentration, especially along the catalytic layer, will decrease. Moving toward current, oxygen molecules blend with H^+ ions progressing from anode to cathode to produce water. Accordingly, the rate of oxygen mass fraction in fuel cell reduces and lieu the rate of water density on cathode side increases. Likewise, water density increases in cathode as well. As water molecules surround H^+ ions and transfer them to cathode through the membrane, water level along fuel cell increases on both cathode side and current direction.

Fig. 17 compares the rate of water mass fraction in fuel cell for various cases.

Fig. 18 displays temperature distribution along fuel cell. Specifically because of excessive activity and highly intense electrochemical reactions in fuel cell, cases A and B have higher temperature value in the comparison with other cases. Moreover, the reaction throughout fuel cell is relatively high due to the short length of fuel cell in cylindrical design. Hence, comparing to volume in cylindrical design, the amount of electric current produced is much higher than Base case.

Fig. 19 shows the liquid water mass fraction in the fuel cell. This parameter indicates the amount of the liquid water at cathode side.

Water density in membrane depends on membrane water density and cathode side. If dryness causes the reduction of membrane water, it will lose its ability to transfer ions

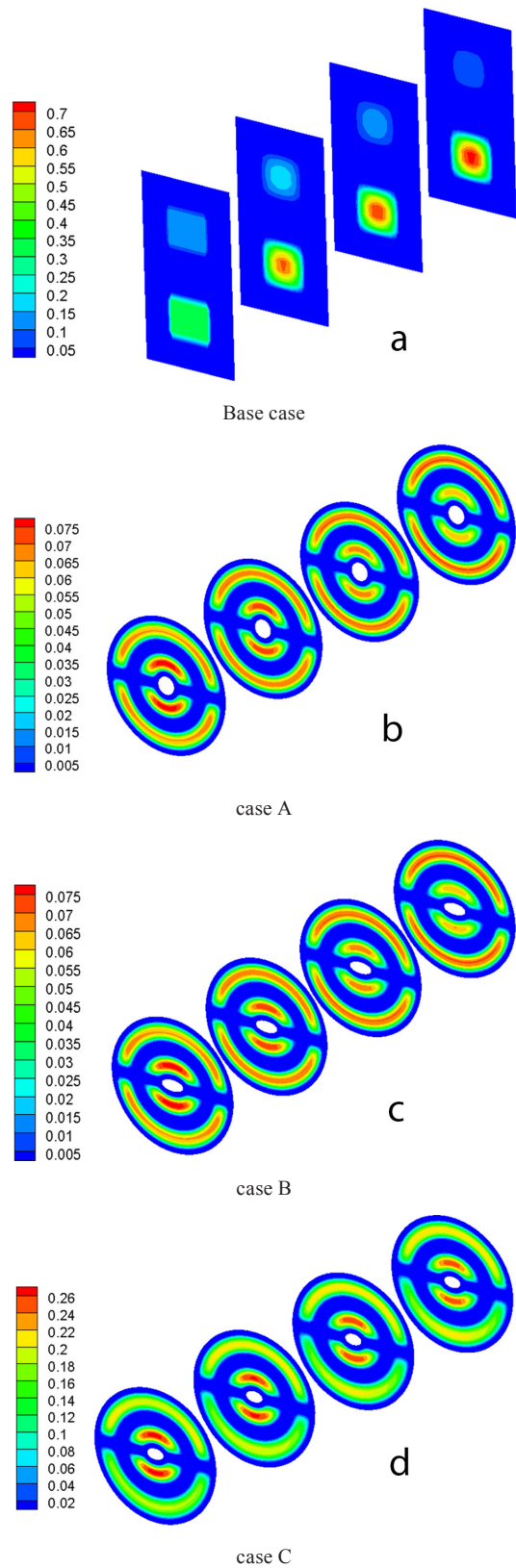
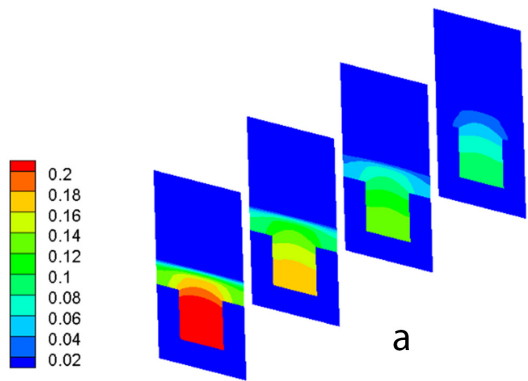
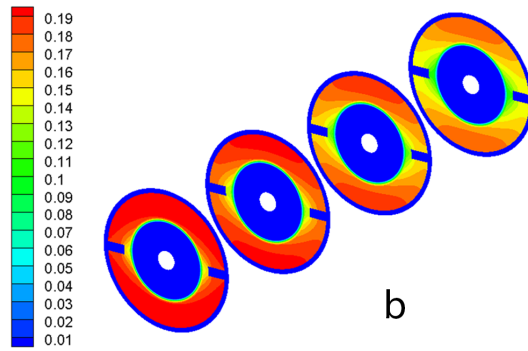


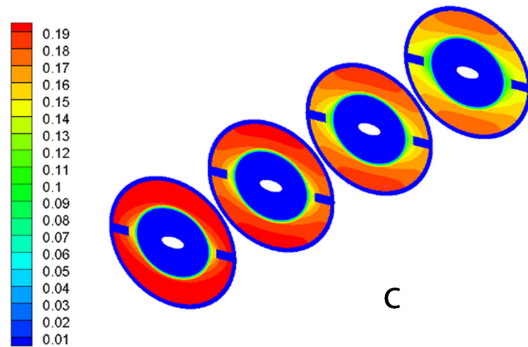
Fig. 15 The Comparison of speed for various cases.



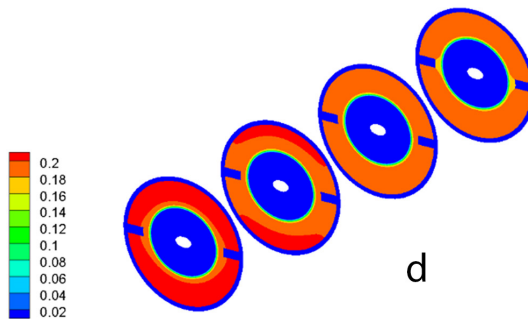
Base case



case A

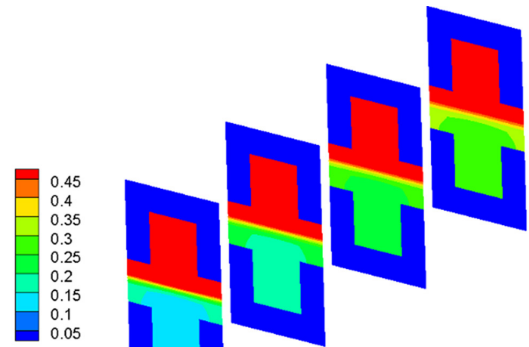


case B

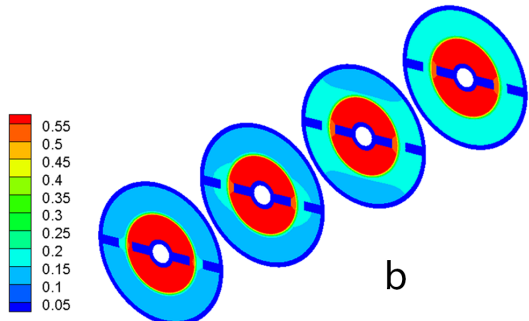


case C

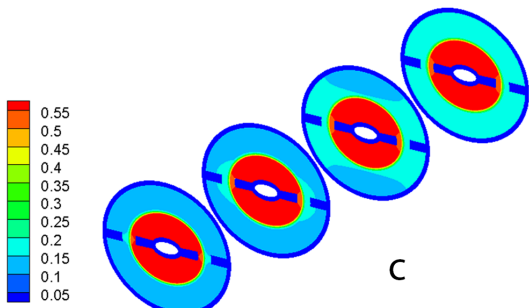
Fig. 16 Comparison of oxygen mass fractions for various cases.



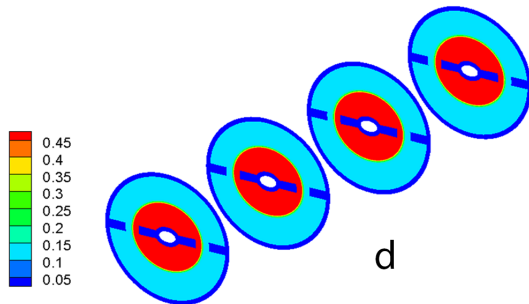
Base case



case A

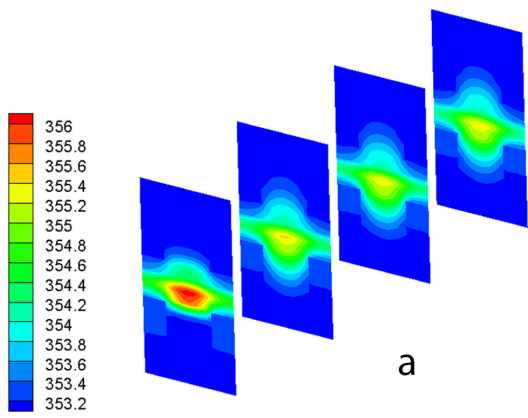


case B

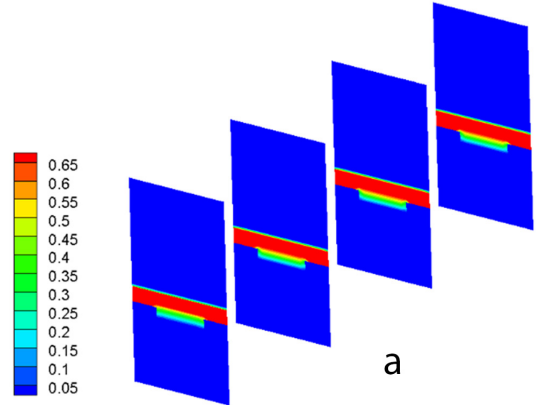


case C

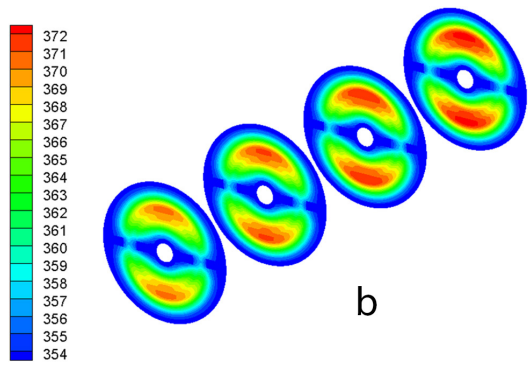
Fig. 17 Comparison of water mass fractions for various cases



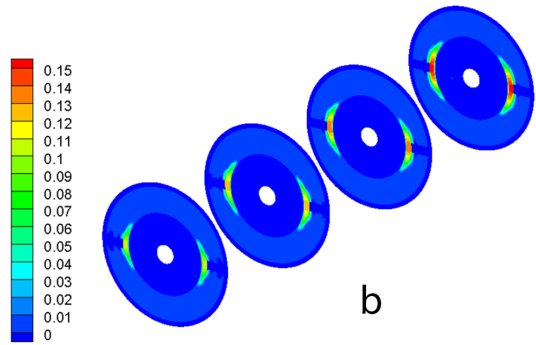
Base case



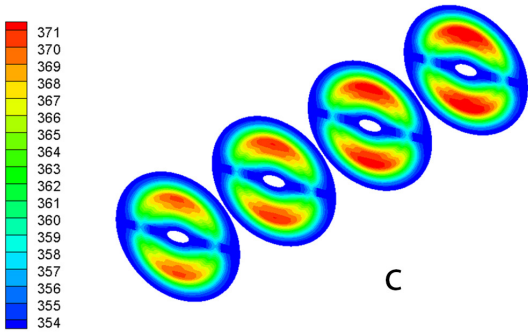
Base case



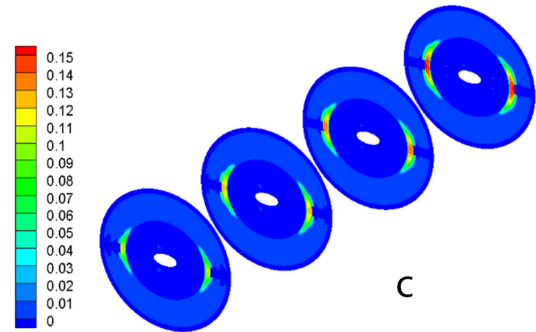
case A



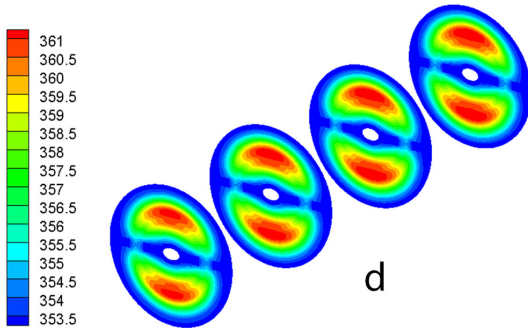
case A



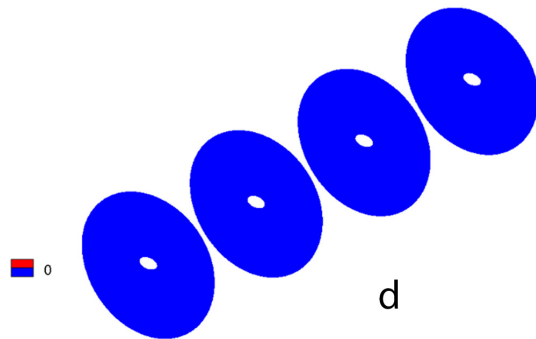
case B



case B



case C



case C

Fig. 18 Comparison of temperature distribution along fuel cell for different cases.

Fig. 19 Comparison of the liquid water mass fraction rate along the fuel cell.

optimally and this in itself lessens polymer fuel cell's performance. However, if multiple reasons such as excessive water accumulation in membrane, cathode gas penetration layer and its porous porosity of permeate layer membrane leads to excessive water density in membrane than fuel cell need in operation voltage, reactive gases will be unable to optimally transmit to reaction areas and participate in reactions continuously. Accordingly, one of the vital parameters in polymer fuel cell performance is the management of optimal amount of water in a fuel cell, especially on cathode side. The less liquid water in fuel cell, the less probability of flood phenomenon on cathode side. Fig. 19 clearly demonstrates the greater amount of liquid water mass fraction in Base case than other cases. This fact increases probability of flood phenomenon and need for water management.

In cases A and B, a very little accumulation of liquid water is seen at the end regions of fuel cell. But this amount of liquid water will have little defective effect on fuel cell performance or its loss. In case C, the amount of liquid water is too low and close zero to lead to any flood performance.

7 Conclusion

Present study introducing a basic model in a three-dimensional, computational fluid dynamics of polymer fuel cell with square gas channels aims to study the effect of overall and incremental geometric changes on polymer fuel cell performance. The geometric changes entail introducing two fuel cells; a polymer with a fragment electrode-membrane set and cylindrical with circular and elliptical cross section represented as A, B and C plans. Initially, a polymer fuel cell with electrode and broken membrane was investigated. The simulations indicate better performance in polymer fuel cell with fragment-electrode-membrane set than Base case. Analytically, better

performance pertains to an effective area increase of reaction, which provokes reactants' efficient and monotonous transmission to reaction regions. The current case is most likely in fragment toward cathode. Likewise, comparing to Base case, new design with a cylindrical shape displays a better performance. Additionally, the cylindrical design provides quite appropriate ground to get optimal and monotonous flow of reactive gases to reaction regions, which stand close to cathode catalytic layer and membrane. Moreover, in cylindrical design, comparing to Base case, the area size of reactor gas passage from gas channel floor to reaction regions is significantly increased. Thereupon, the reactive gases penetrate so much better and quite monotonously into reaction areas. This phenomenon is considerably impressive in case B. Since the length in horizontal part increases, again comparing to case A, the area of reactor passage from channel floor increases as well. Consequently, more gases could get to reaction regions than case A. However, case C displays slight reduction in gas channel input area with the same input mass for reactors. Hence, the speed of anode and cathode gas channels will be higher than the other two. Having kept other parameters stable, velocity increase evinces power increment in momentum displacement compared to mass penetration. Therefore, reduction of mass penetration amount into reaction region leads to significant drop in performance rate. It is worth mentioning that the reactors rate in case B comprises the lowest value and in case C the highest value. On the other hand, in cylindrical fuel cell, the amount of liquid water accumulation on cathode and membrane side is less than Base case causing late flood phenomenon in polymer fuel cell design. Meanwhile, case C carries lower amount of liquid water accumulation (about zero) due to lower water production than the other two, and also higher temperatures than the Base case.

Nomenclature

| | | | |
|-----|---|--------------|---|
| A | Area [m^2] | J | Exchange current density [A m^{-2}] |
| a | Water activity | K | Permeability [m^2] |
| C | Molar concentration [mol m^{-3}] | k | thermal conductivity of gases [$\text{Wm}^{-1}\text{K}^{-1}$] |
| D | Mass diffusion coefficient [$\text{m}^2 \text{s}^{-1}$] | L | Channel length [m] |
| d | Horizontal Radius of ellipse [mm] | P | Pressure [Pa] |
| e | Vertical Radius of ellipse [mm] | R | Universal gas constant [$\text{J mol}^{-1} \text{K}^{-1}$] |
| F | Faraday constant [C mol^{-1}] | S | Source term of equations |
| H | Channel height [m] | T | Temperature [K] |
| h | Deflection height [mm] | \mathbf{u} | Velocity vector |
| I | Local current density [A m^{-2}] | u | Anode and cathode gas channel inlet velocity |
| W | Width | δ | Thickness [m] |

| | |
|-----|-----------------------------------|
| X | Mole fraction |
| x | X direction |
| y | Y direction |
| z | Z direction |
| v | Velocity component in Y direction |
| w | Velocity component in Z direction |

Greek Letter

| | |
|---------------------|--|
| ε_{eff} | Effective porosity |
| ρ | Density [kg m^{-3}] |
| ∇ | vector differential operator |
| ϕ_e | Electrolyte phase potential (varies from -1 to 1) [v] |
| ϕ_{sol} | Solid phase potential [v] |
| ϕ_{mem} | Membrane phase potential [v] |
| μ | Viscosity [$\text{kg m}^{-1}\text{s}^{-1}$] |
| λ | Water content in the membrane |
| ζ | Stoichiometric ratio |
| Φ | Electric potential [V] |

| | |
|----------|---|
| κ | ion conduction in ion metric phase [Sm^{-1}] |
| ψ | Relative humidity [%] |

Subscripts and Superscripts

| | |
|-------|-------------------------------|
| CL | Catalyst Layer |
| GDL | Gas Diffusion Layer |
| an | Anode |
| avg | Average |
| cat | Cathode |
| ch | Channel |
| e | Electrical |
| h | Height |
| in | Inlet |
| K | Chemical species |
| MEA | Membrane electrolyte assembly |
| mem | Membrane |
| sat | saturation |
| sol | Solid |
| u | Velocity |

References

- Ahmadi, N., Rezazadeh, S., Mirzaee, I. "Study the Effect of Various Operating Parameters of Proton Exchange Membrane", Periodica Polytechnica Chemical Engineering, 59(3), pp. 221-235, 2015.
<https://doi.org/10.3311/PPCh.7577>
- He, W. Yi, J. S., Van Nguyen, T. "Two-Phase Flow Model of the Cathode of PEM Fuel Cells Using Interdigitated Flow Fields", Materials, Interfaces, and Electrochemical Phenomena, 46(10), pp. 2053-2064, 2000.
<https://doi.org/10.1002/aic.690461016>
- Kilic, M. S., Korkut, S., Hazer, B. "Electrical Energy Generation from a Novel Polypropylene Grafted Polyethylene Glycol Based Enzymatic Fuel Cell", Analytical Letters, 47(6), pp. 983-995, 2014.
<https://doi.org/10.1080/00032719.2013.860536>
- Grujicic, M., Chittajallu, K. M. "Design and optimization of polymer electrolyte membrane (PEM) fuel cells", Applied Surface Science, 227(1-4), pp. 56-72, 2004.
<https://doi.org/10.1016/j.apsusc.2003.10.035>
- Xing, X. Q., Lum, K. W., Poh, H. J., Wu, Y. L. "Optimization of assembly clamping pressure on performance of proton-exchange membrane fuel cells", Journal of Power Sources, 195(1), pp. 62-68, 2010.
<https://doi.org/10.1016/j.jpowsour.2009.06.107>
- Chang, W. R., Hwang, J. J., Weng, F. B., Chan, S. H. "Effect of clamping pressure on the performance of a PEM fuel cell", Journal of Power Sources, 166(1), pp. 149-154, 2007.
<https://doi.org/10.1016/j.jpowsour.2007.01.015>
- Moreno, N. G., Molina, M. C., Gervasio, D., Pérez Robles, J. F. "Approaches to polymer electrolyte membrane fuel cells (PEMFCs) and their cost", Renewable and Sustainable Energy Reviews, 52, pp. 897-906, 2015.
<https://doi.org/10.1016/j.rser.2015.07.157>
- Amphlett, J. C., Baumert, R. M., Mann, R. F., Peppley, B. A., Roberge, P. R., Harris, T. J. "Performance Modeling of the Ballard Mark IV Solid Polymer Electrolyte Fuel Cell: II. Empirical Model Development", Journal of The Electrochemical Society, 142(1), pp. 9-15, 1995.
<https://doi.org/10.1149/1.2043959>
- Werner, C., Busemeyer, L., Kallo, J. "The impact of operating parameters and system architecture on the water management of a multifunctional PEMFC system", International Journal of Hydrogen Energy, 40(35), pp. 11595-11603, 2015.
<https://doi.org/10.1016/j.ijhydene.2015.02.012>
- Kwon, O.-J., Shin, H.-S., Cheon, S.-H., Oh, B. S. "A study of numerical analysis for PEMFC using a multiphysics program and statistical method", International Journal of Hydrogen Energy, 40(35), pp. 11577-11586, 2015.
<https://doi.org/10.1016/j.ijhydene.2015.03.163>
- Lee, D., Lim, J. W., Nam, S., Choi, I., Lee, D. G. "Gasket-integrated carbon / silicone elastomer composite bipolar plate for high-temperature PEMFC", Composite Structures, 128, pp. 284-290, 2015.
<https://doi.org/10.1016/j.compstruct.2015.03.063>
- Uribe, F. A., Gottesfeld, S., Zawodzinski, T. A. "Effect of Ammonia as Potential Fuel Impurity on Proton Exchange Membrane Fuel Cell Performance", Journal of The Electrochemical Society, 149(3), pp. A293-A296, 2002.
<https://doi.org/10.1149/1.1447221>
- Ticianelli, E. A., Derouin, C. R., Srinivasan, S. "Localization of platinum in low catalyst loading electrodes to attain high power densities in SPE fuel cells", Journal of Electroanalytical Chemistry and Interfacial Electrochemistry, 251(2), pp. 275-295, 1988.
[https://doi.org/10.1016/0022-0728\(88\)85190-8](https://doi.org/10.1016/0022-0728(88)85190-8)

- [14] Yao, K. Z., Karan, K., McAuley, K. B., Oosthuizen, P., Peppley, B., Xie, T. "A Review of Mathematical Models for Hydrogen and Direct Methanol Polymer Electrolyte Membrane Fuel Cells", *Fuel Cells*, 4(1-2), pp. 3-29, 2004.
<https://doi.org/10.1002/face.200300004>
- [15] Natarajan, D., Van Nguyen, T. "A Two-Dimensional, Two-Phase, Multicomponent, Transient Model for the Cathode of a Proton Exchange Membrane Fuel Cell Using Conventional Gas Distributors", *Journal of The Electrochemical Society*, 148(12), pp. A1324-A1335, 2001.
<https://doi.org/10.1149/1.1415032>
- [16] Lin, G., Van Nguyen, T. "A Two-Dimensional Two-Phase Model of a PEM Fuel Cell", *Journal of The Electrochemical Society*, 153(2), pp. A372-A382, 2006.
<https://doi.org/10.1149/1.2142267>
- [17] Lum, K. W., McGuirk, J. J. "Three-dimensional model of a complete polymer electrolyte membrane fuel cell – model formulation, validation and parametric studies", *Journal of Power Sources*, 143(1-2), pp. 103-124, 2005.
<https://doi.org/10.1016/j.jpowsour.2004.11.032>
- [18] Ahmed, D. H., Sung, H. J. "Effects of channel geometrical configuration and shoulder width on PEMFC performance at high current density", *Journal of Power Sources*, 162(1), pp. 327-339, 2006.
<https://doi.org/10.1016/j.jpowsour.2006.06.083>
- [19] Majidifar, S., Mirzaei, I., Rezazadeh, S., Mohajeri Khameneh, P., Oryani, H. "Effect of Gas Channel Geometry on Performance of PEM Fuel Cells", *Australian Journal of Basic and Applied Sciences*, 5(5), pp. 943-954, 2011.
- [20] Ebrahimi, S., Roshandel, R., Vijayaraghavan, K. "Power density optimization of PEMFC cathode with non-uniform catalyst layer by Simplex method and numerical simulation", *International Journal of Hydrogen Energy*, 41(47), pp. 22260-22273, 2016.
<https://doi.org/10.1016/j.ijhydene.2016.07.247>
- [21] Cooper, N. J., Santamaria, A. D., Becton, M. K., Park, J. W. "Investigation of the performance improvement in decreasing aspect ratio interdigitated flow field PEMFCs", *Energy Conversion and Management*, 136, pp. 307-317, 2017.
<https://doi.org/10.1016/j.enconman.2017.01.005>
- [22] Yan, W.-M., Li, H.-Y., Weng, W.-C. "Transient mass transport and cell performance of a PEM fuel cell", *International Journal of Heat and Mass Transfer*, 107, pp. 646-656, 2017.
<https://doi.org/10.1016/j.ijheatmasstransfer.2016.11.075>
- [23] Liu, J. X., Guo, H., Ye, F., Ma, C. F. "Two-dimensional analytical model of a proton exchange membrane fuel cell", *Energy*, 119, pp. 299-308, 2017.
<https://doi.org/10.1016/j.energy.2016.12.075>
- [24] Ahmadi, N., Dadvand, A., Mirzaei, I., Rezazadeh, S. "Modeling of polymer electrolyte membrane fuel cell with circular and elliptical cross-section gas channels: A novel procedure", *International Journal of Energy Research*, 42(8), pp. 2805-2822, 2018.
<https://doi.org/10.1002/er.4069>
- [25] Ahmadi, N., Rezazadeh, S., Dadvand, A., Mirzaei, I. "Modelling of gas transport in proton exchange membrane fuel cells", *Proceedings of the Institution of Civil Engineers - Energy*, 170(4), pp. 163-179, 2017.
<https://doi.org/10.1680/jener.15.00015>
- [26] Gurau, V., Liu, H., Kakaç, S. "Two-dimensional model for proton exchange membrane fuel cells", *AICHE Journal*, 44(11), pp. 2410-2422, 1998.
<https://doi.org/10.1002/aic.690441109>
- [27] Meredith, R. E., Tobias, C. W. "Advances in Electrochemistry and Electrochemical Engineering", 1st ed., Interscience Publishers, New York, USA, 1962.
- [28] Bird, R. B., Stewart, W. E., Lightfoot, E. N. "Transport phenomena", 1st ed., John Wiley & Sons, Inc., New York, USA, 1960.
- [29] Springer, T. E., Zawodzinski, T. A., Gottesfeld, S. "Polymer Electrolyte Fuel Cell Model", *Journal of The Electrochemical Society*, 138(8), pp. 2334-2342, 1991.
<https://doi.org/10.1149/1.2085971>
- [30] Kulikovskiy, A. A. "Quasi-3D Modeling of Water Transport in Polymer Electrolyte Fuel Cells", *Journal of The Electrochemical Society*, 150(11), pp. A1432-A1439, 2003.
<https://doi.org/10.1149/1.1611489>
- [31] Yeo, S. C., Eisenberg, A. "Physical properties and supermolecular structure of perfluorinated ion-containing (nafion) polymers", *Journal of Applied Polymer Science*, 21(4), pp. 875-898, 1977.
<https://doi.org/10.1002/app.1977.070210401>
- [32] Wang, L., Husar, A., Zhou, T., Liu, H. "A parametric study of PEM fuel cell performances", *International Journal of Hydrogen Energy*, 28(11), pp. 1263-1272, 2003.
[https://doi.org/10.1016/S0360-3199\(02\)00284-7](https://doi.org/10.1016/S0360-3199(02)00284-7)
- [33] Patankar, S. "Numerical heat transfer and fluid flow", 1st ed., CRC Press, New York, USA, 1980.